Understanding the self-assembly of charged nanoparticles at the water/oil interface†

François Reincke,[a] Willem K. Kegel,[c] Hao Zhang,[a] Marc Nolte,[a] Dayang Wang,*[a] Daniel Vanmaekelbergh[b] and Helmuth Möhwald[a]

Received 28th March 2006, Accepted 7th June 2006
First published as an Advance Article on the web 19th June 2006
DOI: 10.1039/b604535a

We present a thermodynamic evaluation of the self-assembly of charged nanometer-sized particles at the water/oil interface. The chemical potentials of the nanoparticles in the bulk (aqueous) phase and at the water/oil interface are calculated taking into account interfacial energies, van der Waals interactions, and electrostatic repulsions. An isotherm of the interfacial particle density as a function of the surface charge density on the particles is obtained and compared with experimental results on gold and CdTe nanoparticles self-assembled at the water/heptane interface. Our model provides a semi-quantitative explanation for the spontaneous self-assembly of several types of metallic and semiconducting charged nanoparticles upon reduction of their surface charge.

1. Introduction

Inorganic colloidal nanoparticles have size-dependent, tunable electrical[1–5] and optical[5–8] properties. This has led to a worldwide and still growing interest in their synthesis and further processing. Self-assembly of nanoparticles into two-[9–13] or three-dimensional superlattices[14–16] is a route to create novel opto-electronic materials, in which the interaction between the nanoparticles can be tuned. Usually, *uncharged* dielectric[9] and metallic[10–12] nanoparticles capped with organic molecules are being employed. Controlled evaporation of the solvent or addition of a non-solvent leads to the formation of dense assemblies which can show long-range order, if the size-dispersion is sufficiently narrow. The propensity to self-assemble is due to attractive dispersion forces between the alkyl chains and between the nanoparticle cores.

Self-assembly of *charge-stabilized* colloidal nanoparticles has not been intensively investigated, although the number of publications has been steadily increasing over the last few years.[17–22] Many of these investigations occur at the water/oil interface since it provides an ideal platform for directing their self-assembly. The interfacial assembly of micrometer-sized charge-stabilised particles is well studied. A regular but low density structure of like-charged particles is formed due to electrostatic repulsion between the particles.[23] It was shown that dense layers of micrometer-sized charged colloids[24] or large multivalent ions[25] could be formed after lateral compression. Since these particles are not capped, the dense 2-D layers cannot be compressed reversibly, unlike the uncharged colloidal particles capped with long alkyl chains.[12] It was found that the onset of this 2-D aggregation was favoured by destabilization of the particle by addition of salts[24,26] or surfactants.[27] The formation of 2-D aggregates was also found to depend on the particle three-phase contact angle.[28]

The behaviour of micrometer-sized particles has been described using thermodynamics.[29] The main driving force for the attachment of a colloidal particle to the liquid/liquid or liquid/air interface is a decrease in interfacial energy.[26,30] This decrease depends on the three-phase contact angle θ and the line tension γ_l,[30] the highest attachment energy is found when the particle wets both phases equally, *i.e.* $\theta = 90^\circ$. Usually, the interfacial attachment energy of micrometer sized particles is in the order of $10^6\ kT$; the particles are effectively stuck at the interface.[31] However, nanoparticles with a size below 10 nm have an attachment energy that is comparable to the thermal fluctuation energy kT; thermal fluctuations can detach the nanoparticles from the interface and into the bulk phase. For such small particles the line tension becomes relatively important; a small deviation of a few degrees away from $\theta = 90^\circ$ can already prevent the particles from attaching to the interface.[30] Wetting experiments[20,21] confirmed that a three-phase contact angle of approximately 90° is required to form interfacial layers of gold and silver nanoparticles. Lin *et al*. showed that 3 nm CdSe attached to the toluene/water interface are spontaneously replaced by 5 nm CdSe nanoparticles.[19,22] This suggests that the interfacial self-assembly of nanoparticles have an interesting dynamic character.

In this paper we show that, unlike micrometer-sized particles, nanometer-sized carboxylic acid functionalised nanoparticles with a size smaller than 10 nm can be attached to and detached from the liquid/liquid interface and subsequently redispersed in the aqueous bulk phase by changing the pH. Altering the pH is a convenient way to influence the adsorption[20] and properties[32] of colloids at the interface. The

[a] *Max Planck Institute of Colloids and Interfaces, D-14424 Potsdam, Germany. E-mail: dayang.wang@mpikg-golm.mpg.de; Fax: (+49) 331 567 9202*
[b] *Condensed Matter and Interfaces, Utrecht University, 3508 TA Utrecht, The Netherlands*
[c] *Van't Hoff Laboratory for Physical and Colloid Chemistry, Utrecht University, 3508 TA Utrecht, The Netherlands*
† Electronic supplementary information (ESI) available: Experimental details. See DOI: 10.1039/b604535a

reversibility of such nanoparticle systems makes it well suited to a thermodynamic description. In this article we present a thermodynamic framework, inspired by Paunov *et al.*,[29] providing a basic explanation for the self-assembly of charged nanoparticles at the water/oil interface.[20,21] We compare the calculated surface coverage *versus* particle surface charge density curves with two experimental cases, *i.e.* gold and CdTe nanoparticles. The results promise to open new ways of creating extended structures from charged nanoscale building blocks.

2. Experimental methods

Gold nanoparticles smaller than 16 nm in size were produced by a sodium borohydride reduction of aqueous hydrogen tetrachloroaurate ($HAuCl_4$) solution in the presence of thiol ligands. The molar ratios between $HAuCl_4$ to the ligands were chosen as 1 : 1, 2 : 1 and 4 : 1, yielding nanoparticles with a diameter of 2 nm, 6 nm and 10 nm, respectively. The particle size was determined by means of dynamic light scattering (DLS) and TEM. The capping of 3-mercaptopropionic acid (3-MPA) and 4-mercaptobenzoic acid (4-MBA) yielded Au nanoparticles with similar mean sizes. The polydispersity was about 20% for all solutions. 16 nm citrated-stabilized Au nanoparticles were prepared according to the procedure described by Frens.[33] The citrate was replaced with 4-MBA *via* a ligand exchange reaction. The size polydispersity of the resulting nanoparticles is about 10%. CdTe particles were prepared as described previously.[34]

In glass vials, aqueous solutions of gold nanoparticles were brought into contact with heptane. The pH of the original aqueous solutions was 9 for Au nanoparticles and 10 for CdTe nanoparticles. By carefully adding 1 M HCl while stirring, the pH of the aqueous phase gradually decreased to 2. Vigorous shaking yielded a purple emulsion or thin film between water and heptane. The pH of the aqueous phase was adjusted back to 9 or 10 by addition of 1 M NaOH.

TEM images were obtained by a Zeiss EM 912 Omega microscope at an acceleration voltage of 120 kV. DLS measurements were implemented by a Malvern HPPS 500. UV-Vis absorption spectra were recorded by using a Cary 50 UV-visible spectrophotometer. Contact angle measurements were implemented with a contact angle measuring system G10 apparatus (Krüss, Germany) at ambient temperature. Zeta potential measurements were performed with a Malvern Zetasizer 3000 HS.

Confocal microscopy was performed using a Leica TCS NT SP confocal system (Leica, Germany) equipped with a 40× oil immersion objective with a N.A. of 1.25. Before measurement, the pH of aqueous CdTe nanoparticle solution was adjusted with 1 mM HCl and the ionic strength was set to 1 mM using 0.1 M NaCl. 10 μl of aqueous 3 or 4 nm 3-MPA capped CdTe nanoparticles solution was dropped into a transparent container filled with heptane. After waiting more than 10 minutes, a horizontal section containing the water/heptane interface was imaged with the confocal microscope (see Fig. 5a). The intensities of the interface and aqueous bulk phase were determined from at least 6 images taken from the water/heptane interface at several different positions in the cell.

3. Modeling the self-assembly of charged nanoparticles at the water/oil interface

From experiments it is known that colloidal nanoparticles are either in the bulk (water) phase or at the water/organic interface.[20,21] Therefore we compute the Helmholz free energy for both configurations. We introduce several possibilities for the electrostatic repulsion between the particles, *viz.* direct and indirect Coulomb, and dipole–dipole interactions. By equating the chemical potentials in bulk and at the interface, we then obtain an expression for the system at equilibrium. Since the interparticle interaction is distance-dependent, the 2-D equilibrium density of particles at the interface ϕ_s^{eq} can be derived from this equation. An extended explanation can be found in the electronic supplementary information.†

The chemical potential for charged nanoparticles in the aqueous (bulk) phase

We take the colloidal aqueous (bulk) phase to be sufficiently diluted so that interactions between the particles can be neglected. Also the particles are assumed to be monodisperse, equally charged and spherical. Due to the latter condition only translational degrees of freedom have to be taken into account. Furthermore, we assume a dilute hexagonal ordering of particles at the interface. Wetting experiments showed that the three-phase contact angle of nanoparticles at the water/oil interface is very close to 90°.[20,21] Additionally, Aveyard *et al.* demonstrated that nanometer-sized particles cannot attach to the interface if the contact angle is far away from 90 degrees, due to line tension.[30] Therefore we take the particles to be halfway in the interface. With these assumptions, the bulk chemical potential is found to be:[35]

$$\frac{\mu_{bulk}}{kT} = \ln\left(\frac{v_w}{v_p}\right) + \ln(\phi) + \frac{4\pi R^2 \gamma_{c/w}}{kT} \qquad (1)$$

In this equation, R is the particle radius, $\gamma_{c/w}$ is the interfacial tension between water (solvent) and the colloidal particle, v_w is the water volume, $v_p = 4/3\pi R^3$ is the particle volume, and $\phi = v_p\rho$ (with ρ the particle number density) is the volume fraction of the colloids in the water phase. The first two factors in eqn (1) constitute an ''ideal gas''-like entropic term;[35] the last term of eqn (1) is the free energy of the particle–solvent interface.

According to the Young–Dupré equation $\gamma_{c/w} = \gamma_{c/o}$ if $\theta = 90°$. Eqn (1) predicts that the colloids disperse equally well in the water and organic phases. However, the dispersion of charged nanoparticles in the organic phase has not been seen experimentally.[20,21] At this point we do not have an explanation for this obvious inconsistency. Motivated by the experiments, we will not include the dispersion of particles in the bulk organic phase in our model.

The chemical potential for charged nanoparticles at the water/oil interface

The interactions between particles at the interface cannot (solely) be described by the well-known DLVO theory.[36–38] The chemical potential of a charged nanoparticle at the water/organic interface is dominated by three types of interactions:[36,39]

(i) the energy of the water/organic, water/particle and particle/organic interfaces in the system and the translational entropy of the particles at the interface;

(ii) electrostatic repulsions between the colloids: the direct and screened Coulomb repulsions, and the dipole interactions between the incomplete double layer around the colloids;

(iii) the attractive van der Waals interactions between the colloidal particles adsorbed at the interface.

(i) The chemical potential due to the interfacial tension (assuming $\theta = 90^\circ$) is,

$$\mu_\gamma = 4\pi R^2\gamma_{c/w} - \pi R^2\gamma_{o/w} + 2\pi R\gamma_l \qquad (2)$$

Although the translational entropy of dense systems is extremely difficult to estimate (see *e.g.*, Hoover *et al.*[40]), dynamic light scattering experiments on Au nanoparticles in the colloidal solution and at the interfacial layer showed that the mobility is several orders of magnitude slower than in the aqueous bulk.[41] This suggests that the particles in the interfacial layer of colloids are nearly completely immobilised and only the layers as a whole are free to move. Therefore we choose to neglect the translational entropy altogether.

(ii) In literature there has been debate about the nature of the electrostatic repulsions between charged nanoparticles at air/liquid and liquid/liquid interfaces. Therefore we will discuss several possibilities for the electrostatic repulsion.

First, we will use description based upon a suggestion of Pieranski.[9] Pieranski suggested that since the electrical double layer is only present at the aqueous side of the particle, a nett dipole moment induced by the double layer is present. The chemical potential due the dipole interaction can be written as:

$$\mu_{dipole} = \frac{5z\pi R\sigma^2 L_D^2 y^{\frac{3}{2}}}{16\varepsilon_{dipole}\varepsilon_0} \qquad (3)$$

with σ the measured surface charge density, z the number of nearest neighbours in two dimensions, L_D the Debye length, ε and ε_0 the relative dielectric constant and the permittivity of vacuum, respectively, and $\gamma = \phi_s/\phi_s{}^*$ where $\phi_s^* = \phi_s (r = 2R) = \frac{1}{6}\sqrt{3\pi}$ is the surface fraction of a close-packed monolayer and r the center to center distance between the particles. The surface fraction $\phi_s = N\pi R^2/A_{o/w}$, were $A_{o/w}$ the area of the water/organic interface, is defined similarly to the volume fraction ϕ. Although the dipoles themselves are in the water phase, the dipole interaction partially takes place through the organic phase, due to their proximity to the oil phase. Therefore ε_{dipole} is likely to be a weighted average of the dielectric constant of the aqueous and organic phases.

Robinson and Earnshaw[42] suggested that the colloid/water interface might contain dipolar groups, giving rise to an unscreened dipolar interaction through the oil phase. However, Horozov *et al.*[28] showed that this type of dipolar repulsion can not explain the interactions between micrometer sized silica particles at the water/oil interface. Moreover, the high curvature of nanometer sized particles, relative to their Debye length, means that it is unlikely that a net dipole moment can exist at the colloid/water interface, since the dipole moments mostly cancel each other out due to their different orientations. Therefore we have not included this possibility here.

Second, Aveyard *et al.*[24] showed that unscreened ions can be present at the oil/colloid interface. Since this charge is no longer screened by the aqueous phase, this constitutes a strong long-range Coulomb repulsion between the particles at the interface which takes place through the organic phase:

$$\mu_{coulomb} = \frac{3z\pi R^3\alpha^2\sigma^2\sqrt{y}}{8\varepsilon_{organic}\varepsilon_0} \qquad (4)$$

It is unlikely that the entire surface charge σ is present at the colloid/oil interface, due to transfer of charged species to the water phase. Additionally, some of the charged species could recombine with their counter-ion. Therefore the scaling factor α, which has a value between 0 and 1, is used in eqn (4).

Finally, we will also consider the interaction of the particle double layers through the water phase. We have used a Yukawa style interaction parameter

$$\mu_{Yukawa} = \frac{z\pi R^3\sigma^2}{8\varepsilon_{water}\varepsilon_0}\left(3\sqrt{y} + \frac{2R}{L_D}\right)e^{\frac{2R}{L_D\sqrt{y}}} \qquad (5)$$

(iii) While van der Waals interactions decay as the inverse distance to the power of six for atoms, in the case of colloids this decay is much slower,[43] *i.e.*,

$$\mu_{vdWaals} = -\frac{zH}{12}\left(\frac{y^2}{2(y-1)^2} + y + \ln(1-y)\right) \qquad (6)$$

where H is the Hamaker constant.

Adding all the interfacial contributions (equations (2) through (6)) we obtain the chemical potential of a particle adsorbed at the oil–water interface

$$\frac{\mu_{int}}{kT} = \frac{\pi R^2}{kT}\left(\frac{2\gamma_l}{R} - \gamma_{o/w} + 4\gamma_{c/w}\right) + \mu_{electrostatic} - \frac{zH}{12kT}\left(\frac{y^2}{2(y-1)^2} + y + \ln(1-y)\right) \qquad (7)$$

where $\mu_{electrostatic}$ contains one or more of the electrostatic repulsion terms $\mu_{Coulomb}$, μ_{Yukawa} and μ_{dipole}, eqns (3) through (5), respectively. We will later discuss which term(s) in $\mu_{electrostatic}$ are expected to be dominant.

Equilibrium bulk and surface fraction

Setting $\mu_{bulk} = \mu_{int}$ gives the interfacial density as a function of bulk density, charge density, Hamaker constant, particle size and interfacial tensions. By combining eqns (1) and (7) we see that the contributions containing $\gamma_{c/w}$ cancel. Thus, the equilibrium bulk ϕ^{eq} and surface fraction ϕ_s^{eq} (the superscript 'eq' has been added to distinguish from the non-equilibrium case) follows by numerically solving

$$\frac{\pi R^2}{kT}\left(\frac{2\gamma_l}{R} - \gamma_{o/w}\right) + \mu_{electrostatic} - \frac{zH}{12kT}\left(\frac{y^2}{2(y-1)^2} + y + \ln(1-y)\right) = \ln\left(\frac{\nu_w}{\nu_p}\right) + \ln(\phi^{eq}) \qquad (8)$$

remembering that $\mu_{electrostatic} = f(\phi_s^{eq},\sigma)$.

In fact, ϕ and ϕ_s are related to the initial volume fraction (*i.e.* before adsorption takes place) in the water phase, ϕ_{init}, by

matter conservation:

$$\phi_{\text{init}} = \phi + \frac{4AR}{3V}\phi_s \qquad (9)$$

with V the volume of the aqueous phase, as before. In our case AR/V is always very small compared to ϕ_{init} so that in our calculations we set $\phi \approx \phi_{\text{init}}$.

Equilibrium surface coverage *versus* charge density

Assuming that both dipole and unscreened Coulomb interactions are present, *i.e.* using eqns (3), (4), (8) and (9), we have plotted ϕ_s^{eq} as a function of the nanoparticle surface charge density σ, see Fig. 1, for several nanoparticles with a size below 10 nm. When the electrostatic repulsion between the particles is large, *i.e.* for high values of σ^2/ε, the model predicts an equilibrium surface density at a low value of ϕ_s^{eq}. The equilibrium point is formed by a balance between the interfacial attachment energy, eqn (2), and the interparticle electrostatic repulsion, eqn (4) through (6). In Fig. 1 all curves have been truncated at approximately $\phi_s^{eq} \approx 0.6$. From this point the van der Waals attraction becomes dominant. The form of van der Waals term used, eqn (6), is not correct when particles at the interface are close together (eqn (6) goes to minus infinity when $y = \phi_s/\phi_s^* \rightarrow 1$). Moreover, chemical and steric interactions can occur when the particles nearly meet. Therefore we have chosen to truncate the isotherms at high values of ϕ_s^{eq}.

If a small particle is highly charged (large surface charge density σ) the interfacial coverage ϕ_s^{eq} is low, see the solid line in Fig. 1 (see also Pieranski[9]). If the surface charge density σ is decreased, *e.g.* by changing the pH of the aqueous solution,[44] the electrostatic interactions between the particles at the interface decrease. As a result, ϕ_s^{eq} increases steeply until a critical surface charge density is reached. Below this critical surface charge density eqn (8) no longer has a solution, due to the problems explained above. In this case, the interface is likely to be completely filled with particles since $\mu_{\text{int}} < \mu_{\text{bulk}}$, as seen experimentally. Aggregation of particles in the aqueous bulk phase may also occur. In theory, when the surface charge density is raised to its original value the system should return to its original state, *i.e.* the nanoparticles should detach from the interface and redisperse in the aqueous bulk phase. In this case, we say that the interfacial attachment is reversible.

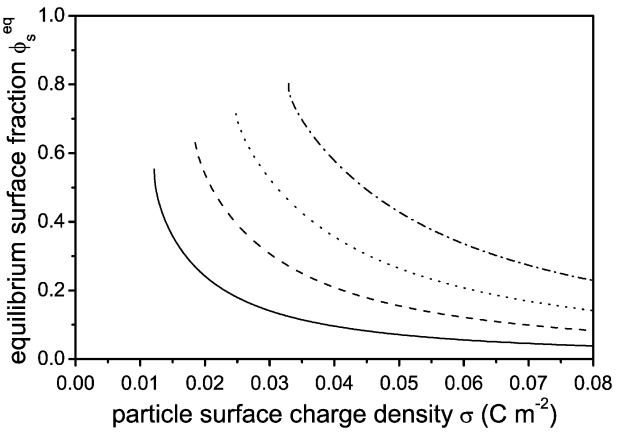

Fig. 1 Results of the model calculations for charged nanoparticles self-assembled at the water/heptane interface. Using eqn (8), the equilibrium surface fraction is plotted as a function of surface charge density. The electrostatic repulsion between the nanoparticles in the interface was assumed to be caused by the dipole repulsion μ_{dipole} due to incomplete double layers around the particles (eqn (3)), *i.e.* $\mu_{\text{electrostic}} = \mu_{\text{dipole}}$ (eqn (7)). The particle diameter (2R) was chosen as 1 (solid), 2 (dashed), 4 (dotted), and 8 nm (dash-dotted). Other values used were $z = 6$, $L_D = 9.7$ nm, $\gamma_{o/w} = 50$ mN m^{-1}, $\gamma_l = 10^{-12}$ N, $\phi_{\text{init}} = 10^{-5}$, H = 3.4×10^{-20} J (the value for CdS in H_2O, ref. 51), $\alpha = 0.1$, $T = 298$ K, $\varepsilon_{\text{organic}} = 2$, and $\varepsilon_{\text{dipole}} = 41$. Since the particle is half-way in the interface, the dipole interaction was assumed to equally interact through the water and heptane interface, therefore $\varepsilon_{\text{dipole}}$ was set to 41.

Big particles adsorb more strongly to the interface than small particles, due to the larger interfacial attachment energy (see eqn (1)). Hence, for constant values of σ, big particles reach a higher interfacial coverage ϕ_s^{eq} than small particles (compare the solid and dash-dotted line in Fig. 1). Also the critical surface charge density is larger for bigger particles. Therefore a higher surface charge is required to remove them from the interface. However, there is a maximum amount of charge that can be placed on an individual nanoparticle, which depends on the particle composition and capping. Hence, there is a maximum size at which reversible interfacial attachment is possible.

Previously we have accepted three possibilities for the electrostatic repulsion between particles at the interface, *viz.* the direct and indirect Coulomb, and dipole interactions, eqns (3) through (5). μ_{Yukawa}, eqn (5), is, at most, on the order of several kT, whereas the other electrostatic interactions are easily on the order of several tens of kT. Hence, the direct Coulombic repulsion through the water phase is negligible with respect to the other electrostatic interactions and will be neglected.

Remembering that $y = \phi_s/\phi_s^* \propto R^2$ it can be seen that both the direct Coulomb and the dipole interactions scale with R^4. Thus, no distinction can be made between the two interactions on the basis of the size-dependence of the isotherm. However, there is a way to discriminate between these two types of repulsions. Since $\mu_{\text{dipole}} \propto L_d^{-2}$, see eqn (3), the dipole interaction decreases as the ionic strength of the aqueous solvent increases. In contrast, μ_{coulomb} (eqn (4)) is independent of the ionic strength. For an extended discussion about the forces between particles at the interface, see for instance, ref. 28,36 and 45

To conclude our discussion of this model, it is interesting to note that the factors associated with the bulk phase are often negligible compared to the factors associated with the interface. Therefore the assembly of particles cannot be described with standard isotherms, such as the Langmuir isotherm. For instance, the chemical potential of the bulk μ_{bulk} has a logarithmic dependence on the bulk fraction ϕ (see eqn (1)), whereas the chemical potential of the interface μ_{int} depends on ϕ_s to the power of 3/2, see eqns (3) and (7).

4. Experiments on gold nanoparticles at the water/heptane interface

We have recently shown that citrate capped gold nanoparticles can self-assemble into a randomly packed colloidal monolayer at the water/heptane interface after addition of ethanol.[20] The

interface becomes increasingly populated as the concentration of ethanol increases. Electrophoresis measurements showed that ethanol reduced the particle surface charge density, most likely due to competitive adsorption with citrate on the gold nanoparticles. Unfortunately, the addition of ethanol also changes the surface chemistry of the gold nanoparticles. To avoid this we attempted to assemble 3-mercaptopropionic acid (3-MPA) and 4-mercaptobenzoic acid (4-MBA) capped gold nanoparticles at the water/heptane interface.

The pH of the original aqueous gold nanoparticle solutions was 9, which is above the pK_as of 3-MPA and 4-MBA. This means that the acid groups of the capping on the Au nanoparticles are deprotonated and the particles are negatively charged. This was confirmed by zeta potential measurements (see Fig. S1 from the ESI)†. When 6 nm gold nanoparticle solutions, capped with either 4-MBA or 3-MPA, were brought into contact with heptane no interfacial attachment of the nanoparticles was observed at the water/heptane interface. The presence of nanoparticles in the aqueous phase was evidenced by its red colour (left vials in Fig. 2 and S2†). The pH of the aqueous Au nanoparticle solutions was gradually adjusted to 2 by careful addition of 1 M HCl. At this pH 3-MPA and 4-MBA are protonated and the particles are uncharged (see Fig. S1†). After vigorous shaking the aqueous phase became completely colourless and a purple coloured emulsion, consisting of millimetre sized droplets, was present between the two phases (middle vials in Fig. S2†). This emulsion slowly dissipated over 1 h, leading to a thin film at the water/heptane interface. This thin film not only resides at the water/heptane interface but also climbs up the heptane/hydrophilic glass interface, exhibiting a purple colour in transmission (middle vial in Fig. 2), as reported previously.[20,21,46] The formation of this interfacial layer was attributed to Marangoni flow.[46] Transmission electron microscopy (TEM) imaging confirmed that a randomly and densely packed monolayer of Au nanoparticles was formed at the water/heptane interface. Few nanoparticles were detected in both the heptane and bulk water phases. When the pH of the aqueous phase was adjusted back to 9 the water phase turned red, similar to the original solutions (right vials in Fig. 2 and S2†). This suggests that the interfacial self-assembly of 6 nm Au nanoparticles is reversible. Similar phenomena were observed using differently sized nanoparticles with dimensions of 2 and 10 nm. The interfacial self-assembly of 16 nm Au nanoparticles was also triggered by lowering the pH of the aqueous phase (Fig. 2). Once they self-assembled at the water/heptane interface, however, they remained attached at the interface despite further variations of the surrounding pH (Fig. 2), reminiscent of micron-sized particles.[47] The removal of micrometer-sized microgel,[48] nanocomposite[49] and polymer-coated[50] particles from the water/oil interface upon a lowering of the pH was indirectly evidenced by the breaking of the emulsions stabilized by these particles. However, as no direct evidence was given that the particles redisperse into one of the bulk phases it is unclear whether the particles truly desorb or appear to desorb as they expand with decreasing pH.

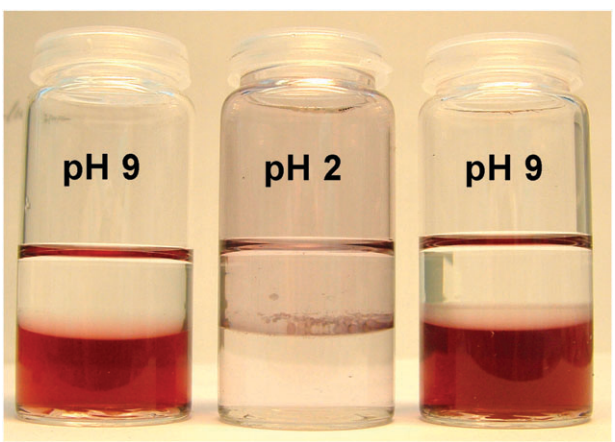

Fig. 2 Photographs of glass vials containing aqueous solutions (bottom) of 4-MBA capped Au nanoparticles with a mean size of 6 nm in contact with heptane (top). The initial aqueous solution of the nanoparticles in the glass vials was red in colour with pH 9 (left). By adding 1 M HCl, the pH of the nanoparticle aqueous solutions was gradually decreased to 2 (middle). After vigorous shaking and storing for 1 h, the thin film of Au nanoparticles, formed at the water/heptane interface, climbed up and coated the interface between heptane and the hydrophilic wall of the glass vial. This film shows a purple transmittance colour. On the right, the pH values of the aqueous solutions were adjusted back to 9 by carefully adding 1 M NaOH. The original colour returned to the aqueous phase, suggesting the redispersion of the nanoparticles in water.

The plasmon absorption of Au nanoparticles provides an efficient *in situ* measurement to monitor the process of nanoparticle self-assembly at the water/heptane interface and the redispersion of nanoparticles in water. In the absence of aggregation or ripening of the particles, the absorption intensity in the aqueous phase is inversely proportional to the amount of nanoparticles at the interface. Fig. 4 reveals that the amount of Au nanoparticles in the aqueous phase changes little until pH 4, which is the pK_a of 3-MPA or 4-MBA. When the pH is lower than 4, the amount of nanoparticles in the aqueous phase dramatically decreases to nearly zero, suggesting that all nanoparticles are located at the water/heptane interface. In the case of nanoparticles with mean sizes smaller than 10 nm, as shown in Fig. 4a, the absorption in the aqueous phase gradually recovered when the pH increased, consistent with Fig. 2 and S2.† By contrast, in the case of 16 nm nanoparticles, the absorption in the aqueous phase was still undetectable, consistent with Fig. 3. This demonstrates the pH switchable interfacial self-assembly only for Au nanoparticles with a size less than 10 nm.

As shown in Fig. 4b, the recovered plasmon absorption of 3-MPA nanoparticles in the aqueous phase has a stronger intensity compared to the original nanoparticles, probably due to coalescence of nanoparticles. In comparison, the benzene ring of 4-MBA provides a better steric stabilization, thus efficiently suppressing the coalescence of their capped Au nanoparticles during the pH cycle and in turn showing a better reversibility even for 10 nm nanoparticles (Fig. 4a). TEM imaging indicated that the size and shape of the Au nanoparticles was little changed before and after self-assembly at the interface (Fig. S3†). The pH-switchable interfacial self-assembly of 4-MBA capped Au nanoparticles with mean sizes less than 10 nm can be repeated at least two times with little change in the apparent colour of the aqueous phase. Further

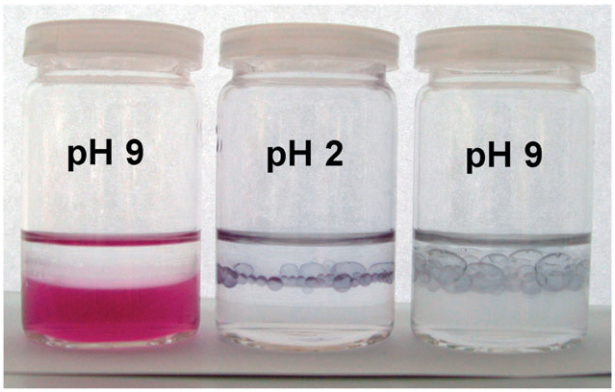

Fig. 3 Photographs of glass vials containing aqueous solutions (bottom) of 4-MBA capped Au nanoparticles with a mean size of 16 nm in contact with heptane (top). The initial aqueous solution of the nanoparticles in the glass vials was red-purple (b.) in colour with pH 9 (left). By adding 1 M HCl, the pH of the nanoparticle aqueous solutions was gradually decreased to 2 (middle). After vigorous shaking and storing for 1 h, the thin film of Au nanoparticles, formed at the water/heptane interface, climbed up and coated the interface between heptane and the hydrophilic wall of the glass vial. This film shows a blue transmittance colour. On the right, the pH values of the aqueous solutions were adjusted back to 9 by carefully adding 1 M NaOH. Unlike the 6 nm gold nanoparticles (Fig. 2) the thin films of 16 nm nanoparticles remained at the interface.

cycling of the pH led to a visible colour change, from red to purple or blue, indicating substantial coalescence of Au nanoparticles. However, a large fraction of the nanoparticles can

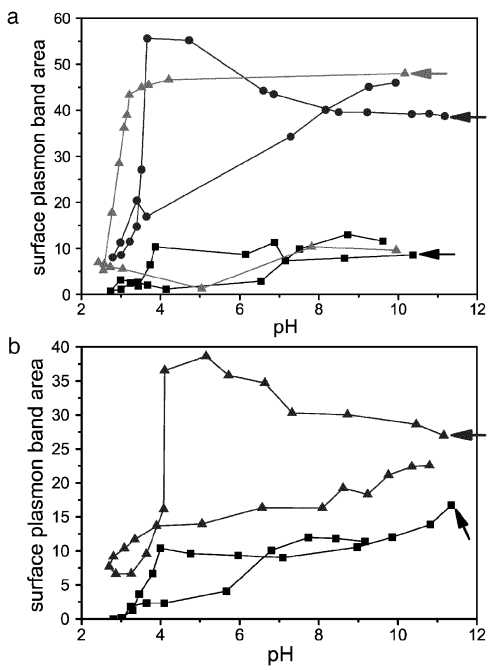

Fig. 4 Plot of the areas of the plasmon absorption bands of Au nanoparticles, capped with 4-MBA (a) and 3-MPA (b), against the pH of the aqueous phase during a pH cycle. The sizes of the nanoparticles used are 2 nm (■), 10 nm (●) and 16 nm (▲). The plasmon absorption bands obtained from UV-Vis spectra were fit by Gaussian curves. The arrows indicate the initial values of the plasmon absorption band areas of Au nanoparticles in the aqueous phases.

be redispersed in the aqueous phase, as evidenced by the colour of the aqueous phase (Fig. S4†).

In Fig. 4 a recovery hysteresis of Au nanoparticles in the aqueous phase can be observed in every measurement. Prior to measurement of the absorption spectra the aqueous phases were dialysed against water to achieve a similar ionic strength before and after the pH adjustment. However, this control experiment showed a similar hysteresis profile of Au nanoparticle recovery. Thus, the hysteresis is not due to variation of the ionic strength. Currently, the origin of this hystersis remains unclear.

5. Confocal microscopy experiments on CdTe nanoparticles at the water/heptane interface

Encouraged by these results, we attempted to self-assemble 3-mercaptopropionic acid capped CdTe nanoparticles at the water/heptane interface. Just like 3-MPA capped gold nanoparticles, the surface charge of the nanoparticle can be varied by varying the pH.[44] The 4 nm CdTe nanoparticles, capped with 3-mercaptopropionic acid (3-MPA), can be attached to the interface by lowering the pH, compare Fig. S7† left and middle vials. When the pH is raised again the particles detach from the interface and redisperse into the organic phase, see Fig. S7† right vial. The advantage of luminescent semiconducting nanoparticles, such as CdTe, is that the interfacial attachment can be monitored by confocal microscopy.[19,22] Images were taken from the water/heptane interface confocal microscope using the setup shown in Fig. 5a. At high pH the particles are dispersed in the aqueous phase, see Fig. 5b. Upon lowering the pH to approximately 5, the particles partially adsorb to the interface, see Fig. 5c. After 20 min no change was observed, indicating that an equilibrium state has been reached at pH = 5. When the pH is decreased even further, see Fig. 5d, all particles go to the interface.

The zeta potential of the aqueous CdTe solution was measured as function of pH, see Fig. 6a. Strangely, the zeta potential of the larger, 4 nm, particles is smaller than that of the 3.3 ones. The surface charge density σ was calculated using the Hückel equation

$$\zeta = \frac{3}{2}\frac{\eta u}{\varepsilon\varepsilon_0} \quad \text{with} \quad u = \frac{\sigma A}{6\pi\eta R} \tag{10}$$

where ζ is the zeta potential, η the viscosity, u the electrophoretic mobility, and A the particle surface area.

Using eqn (10), the relative intensity of the interface with respect to the bulk, derived from confocal images, is plotted against surface charge density σ, see Fig. 6b. The calculated surface charge densities are in reasonable agreement with literature data on TGA capped CdTe nanoparticles.[44] At a surface charge of 0.01 C m^{-2}, the water/oil interface is scarcely populated. As the charge density is decreased from 0.01 to 0.008 C m^{-2} the interface becomes more and more populated. It was found that the amount of CdTe nanoparticles attached to the interface increases with increasing ionic strength. The interaction between particles at the interface is therefore most likely dipolar in nature, as described in eqn (3). Comparing the experimental data with the theoretical curve, such as in Fig. 1, shows that the shape of the curve in Fig. 6b follows the low-

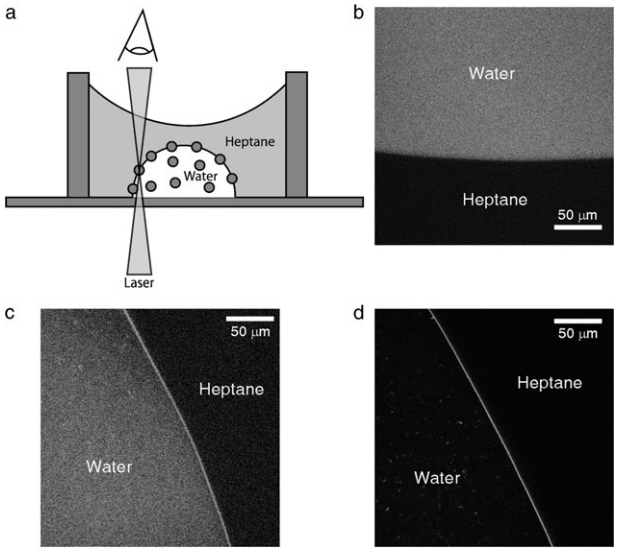

Fig. 5 Confocal images (b. through d.) of an aqueous solution of 3-mercaptopropionate capped CdTe nanoparticles in contact with heptane. In scheme a. the setup used to make the confocal images is depicted. The pH of the aqueous phase was 9.4 (b.), 5.8 (c.) and 4.4 (d.). As the pH is lowered more CdTe particles are driven to the interface until the aqueous phase is completely empty.

density branch of the model well, although the particle charge at which interfacial attachment occurs is approximately 2 times higher than measured with the CdTe nanoparticles.

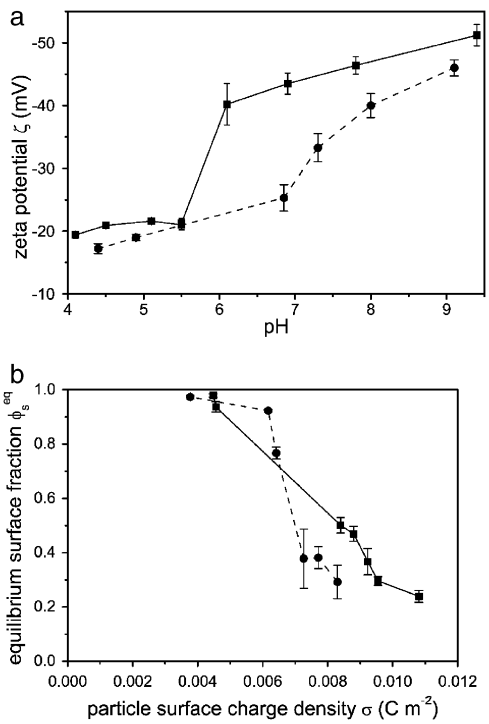

Fig. 6 (a) Plot of the zeta potential of 3 nm (■) and 4 nm (●) 3-MPA capped CdTe nanoparticles as a function of pH. (b) Relative luminescence intensity of the water/heptane interface with respect to the aqueous bulk plotted against the particle surface charge density σ. The luminescence data were derived from confocal images, see Fig. 5. The aqueous bulk contained 3 nm (■) and 4 nm (●) 3-MPA capped CdTe nanoparticles.

We were not expecting a quantitative agreement with the model due to the crude assumptions in the model, in particular the contact angle equal to 90° and pairwise addition of the electrostatic interactions between the particles at the water/oil interface. Both assumptions would overestimate the surface charge density σ required to reach a certain equilibrium density ϕ_s^{eq}.

6. Conclusions

We have theoreticaly and experimentally investigated the self-assembly of charge-stabilised colloidal nanoparticles at the water/oil interface upon gradual variation of their surface charge density. When the particle is highly charged (large surface charge density σ), for example at high pH, the interfacial coverage ϕ_s^{eq} is low; the particles remain in the aqueous bulk phase. Aqueous solutions of 3-MPA capped Au and CdTe nanoparticles in contact with heptane do not show any visible attachment to the water/oil interface. As the surface charge density σ is decreased, ϕ_s^{eq} increases exponentially and the nanoparticles attach to the interface. By lowering the pH, the surface charge density of gold and CdTe nanoparticles is decreased according to the protonation of the capping ligands, thus leading to self-assembly at the interface. Upon an increase of σ, the surface coverage ϕ_s^{eq} decreases dramatically for small particles, allowing for redispersion of the nanoparticles in the aqueous bulk phase. This decrease does not occur for large nanoparticles. Experimentally we demonstrate that reversible interfacial attachment occurs with 4-MBA capped gold nanoparticles with a size smaller than 10 nm.

In our model no assumptions were made about the particle or capping composition. The model should therefore be generally applicable, at least for a qualitative understanding. This is underlined by the fact that nanoparticles composed of two very different core materials, gold and CdTe, show very similar behaviour at the water/heptane interface. The reversibility of interfacial attachment combined with the control over the interfacial density will, in our view, stimulate further nanotechnological research and should open up pathways for creating novel devices with biomimetic structures and functions.

Acknowledgements

We thank Arnout Imhof (Physics & Astronomy, Utrecht University) and Erik Edwards (Colloid and Interface, Max Planck) for helpful discussions. We also thank Heidemarie Zastrow (Colloid and Interface, Max Planck), Hans Meeldijk (Cell Biology, UU) and Stephan Zevenhuizen (Condensed Matter, UU) for technical support.

References

1 R. S. Ingram, M. J. Hostetler, R. W. Murray, T. G. Schaaff, J. T. Khoury, R. L. Whetten, T. P. Bigioni, D. K. Guhrie and P. N. First, *J. Am. Chem. Soc.*, 1997, **119**, 9279.
2 R. P. Andres, T. Bein, M. Dorogi, S. Feng, J. I. Henderson, C. P. Kubiak, W. Mahoney, R. G. Osifchin and R. Reifenberger, *Science*, 1996, **272**, 1323.

3 S. Chen, R. S. Ingram, M. J. Hostetler, J. J. Pietron, R. W. Murray, T. G. Schaaff, J. T. Khoury, M. M. Alvarez and R. L. Whetten, *Science*, 1998, **280**, 2098.
4 M. Y. Han, L. Zhou, C. H. Queck, S. F. Y. Li and W. Huang, *Chem. Phys. Lett*., 1998, **287**, 47.
5 D. Davidovic and M. Tinkham, *Phys. Rev. Lett*., 1999, **83**, 1644.
6 J. A. A. J. Perenboom, *Phys. Rev*., 1981, **78**, 173.
7 S. Link and M. A. El-Sayed, *J. Phys. Chem. B*, 1999, **103**, 4212.
8 G. Mie, *Ann. Phys*., 1908, **25**, 25.
9 P. Pieranski, *Phys. Rev. Lett*., 1980, **45**, 569–572.
10 M. Brust, M. Walker, D. Bethell, D. J. Schiffrin and R. Whyman, *J. Chem. Soc., Chem. Commun*., 1994, 801.
11 J. R. Heath, C. M. Knobler and D. V. Leff, *J. Phys. Chem. B*, 1997, **101**, 189.
12 G. Markovich, C. P. Collier and J. R. Heath, *Phys. Rev. Lett*., 1998, **80**, 3807.
13 C. J. Kiely, J. Fink, M. Brust, D. Bethell and D. J. Schiffrin, *Nature*, 1998, **396**, 444–446.
14 S. Yoshimura and S. Hashisu, *Prog. Colloid Polym. Sci*., 1983, **68**, 59–70.
15 S. Hashisu and S. Yoshimura, *Nature*, 1980, **283**, 188–189.
16 P. C. Ohara, D. V. Leff, J. R. Heath and W. M. Gelbart, *Phys. Rev. Lett*., 1995, **75**, 3466–3469.
17 A. Kumar, P. Mukherjee, A. Guha, S. D. Adyantaya, A. B. Mandale, R. Kumar and M. Sastry, *Langmuir*, 2000, **16**, 9775–9783.
18 A. Kumar, S. Mandal, S. P. Mathew, P. R. Selvakannan, A. B. Mandale, R. V. Chaudhari and M. Sastry, *Langmuir*, 2002, **18**, 6478–6483.
19 Y. Lin, H. Skaff, T. Emrick, A. D. Dinsmore and T. P. Russell, *Science*, 2003, **299**, 226–229.
20 F. Reincke, S. G. Hickey and W. K. Kegel, *Angew. Chem., Int. Ed*., 2004, **43**, 458–462.
21 H. Duan, D. Wang, D. G. Kurth and H. Möhwald, *Angew. Chem., Int. Ed*., 2004, **43**, 5639–5642.
22 Y. Lin, A. Boker, H. Skaff, D. Cookson, A. D. Dinsmore, T. Emrick and T. P. Russell, *Langmuir*, 2005, **21**, 191–194.
23 M. G. Nikolaides, A. R. Bausch, M. F. Hsu, A. D. Dinsmore, M. P. Brenner and D. A. Weitz, *Nature*, 2002, **420**, 299–301.
24 R. Aveyard, J. H. Clint, D. Nees and V. N. Paunov, *Langmuir*, 2000, **16**, 1969–1979.
25 N. Cuvillier and F. Rondelez, *Thin Solid Films*, 1998, **329**, 19–23.
26 D. F. Williams and J. C. Berg, *J. Colloid Interface Sci*., 1992, **152**, 218–229.
27 R. Aveyard, J. H. Clint, D. Nees and N. Quirke, *Langmuir*, 2000, **16**, 8820–8828.
28 T. S. Horozov, R. Aveyard, J. H. Clint and B. P. Binks, *Langmuir*, 2003, **19**, 2822–2829.
29 V. N. Paunov, B. P. Binks and N. P. Ashby, *Langmuir*, 2002, **18**, 6946–6955.
30 R. Aveyard and J. H. Clint, *J. Chem. Soc., Faraday Trans*., 1996, **92**, 85–89.
31 S. Levine and B. D. Bowen, *Colloids Surf*., 1991, **59**, 377.
32 B. P. Binks and J. A. Rodrigues, *Angew. Chem., Int. Ed*., 2005, **44**, 441–444.
33 G. Frens, *Nature (Phys. Sci.)*, 1973, **241**, 20–22.
34 H. Zhang, Z. Zhou, B. Yang and M. Gao, *J. Phys. Chem. B*, 2003, **107**, 8–13.
35 H. Reiss, W. K. Kegel and J. Groenewold, *Ber. Bunsen-Ges. Phys. Chem*., 1996, **100**, 279.
36 F. Martinez-Lopez, M. A. Cabrerizo-Vilchez and R. Hidalgo-Alvarez, *J. Colloid Interface Sci*., 2000, **232**, 303.
37 E. J. Verwey and J. T. G. Overbeek, *Theory of the Stability of Lyophobic Colloids*, Elsevier, Amsterdam, The Netherlands, 1948.
38 A. Moncho-Jorda, F. Martinez-Lopez, A. E. Gonzalez and R. Hidalgo-Alvarez, *Langmuir*, 2002, **18**, 9183–9191.
39 F. Ghezzi and J. C. Earnshaw, *J. Phys.: Condens. Matter*, 1997, **9**, L517–L523.
40 W. G. Hoover and F. H. Ree, *J. Chem. Phys*., 1968, **49**, 3609–3617.
41 F. H. Reincke, PhD thesis, University of Utrecht, 2004.
42 D. J. Robinson and J. C. Earnshaw, *Langmuir*, 1993, **9**, 1436–1438.
43 E. J. W. Verwey and J. T. G. Overbeek, *Theory of stability of lyophobic colloids*, Dover, NY, 1999.
44 A. A. Yaroslavov, V. A. Sinano, A. A. Efimova, E. G. Yaroslavova, A. A. Rakhnyanskaya, Y. A. Ermakov and N. A. Kotov, *J. Am. Chem. Soc*., 2005, **127**, 7322–7323.
45 A. J. Hurd, *J. Phys. A*, 1985, **18**, L1055–L1060.
46 K. S. Mayya and M. Sastry, *Langmuir*, 1999, **15**, 1902–1904.
47 B. P. Binks, *Curr. Opin. Colloid Interface Sci*., 2002, **7**, 21–41.
48 T. Ngai, S. H. Behrens and H. Auweter, *Chem. Commun*., 2005, 331–333.
49 S. Fujii, E. S. Read, B. P. Binks and S. P. Armes, *Adv. Mater*., 2005, **17**, 1014–1018.
50 J. I. Amalvy, S. P. Armes, B. P. Binks, J. A. Rodrigues and G. F. Unali, *Chem. Commun*., 2003, 1826–1827.
51 L. Bergstrom, *Adv. Colloid Interface Sci*., 1997, **70**, 125.